Neuron, Volume
Supplementary Information

Contact repulsion controls the dispersion and final distribution of Cajal-Retzius cells

Verona Villar-Cerviño, Manuel Molano-Mazón, Timothy Catchpole, Miguel Valdeolmillos, Mark Henkemeyer, Luis M. Martínez, Víctor Borrell, Oscar Marín

SUPPLEMENTAL FIGURES

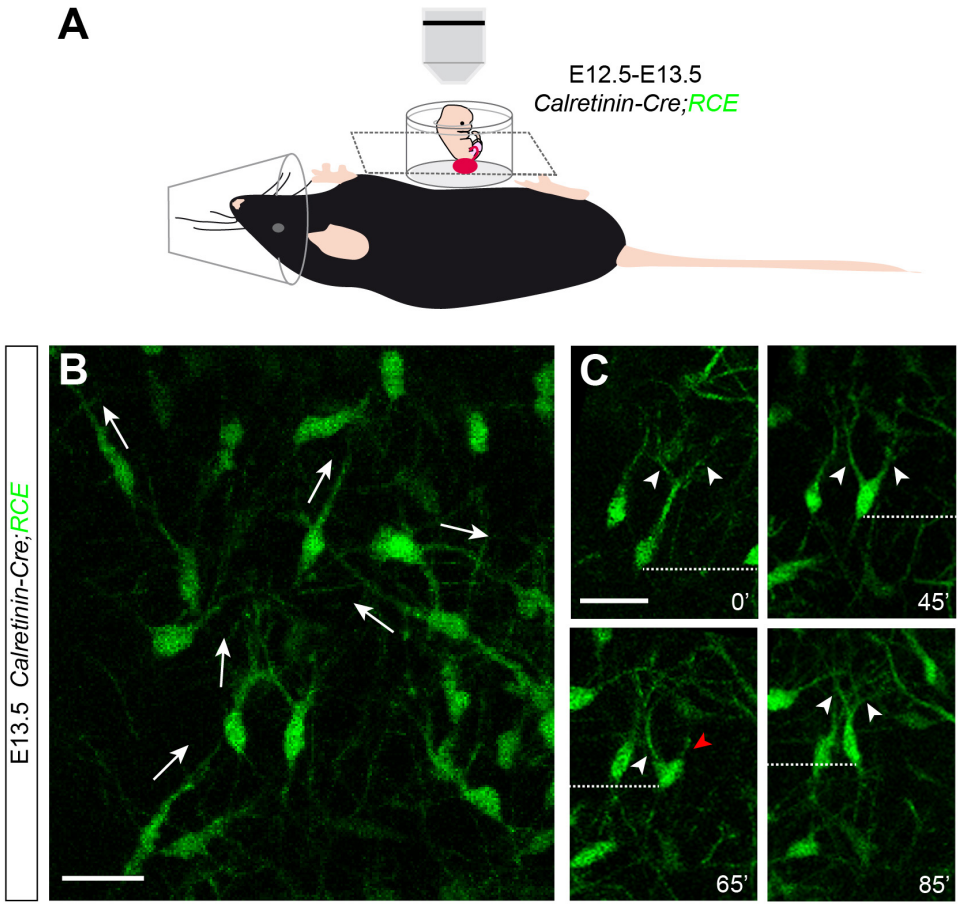

Figure S1. Imaging CR cell migration in vivo.
(A) Schematic of experimental design.
(B) Image of the cortical surface of a E13.5 Calretinin-Cre;RCE mouse embryo showing CR cells (green) oriented in multiple directions (arrows).

(C) Time-lapse sequence of GFP CR cells migrating through the cortical surface. Note that CR cells display a branched leading process, and that they change direction by selecting one of the leading process branches during the course of migration. A dashed line marks the relative position of the soma. White arrowheads point to the leading process. A red arrowhead marks retraction of a leading process branch.
Scale bar equals 50 μm.

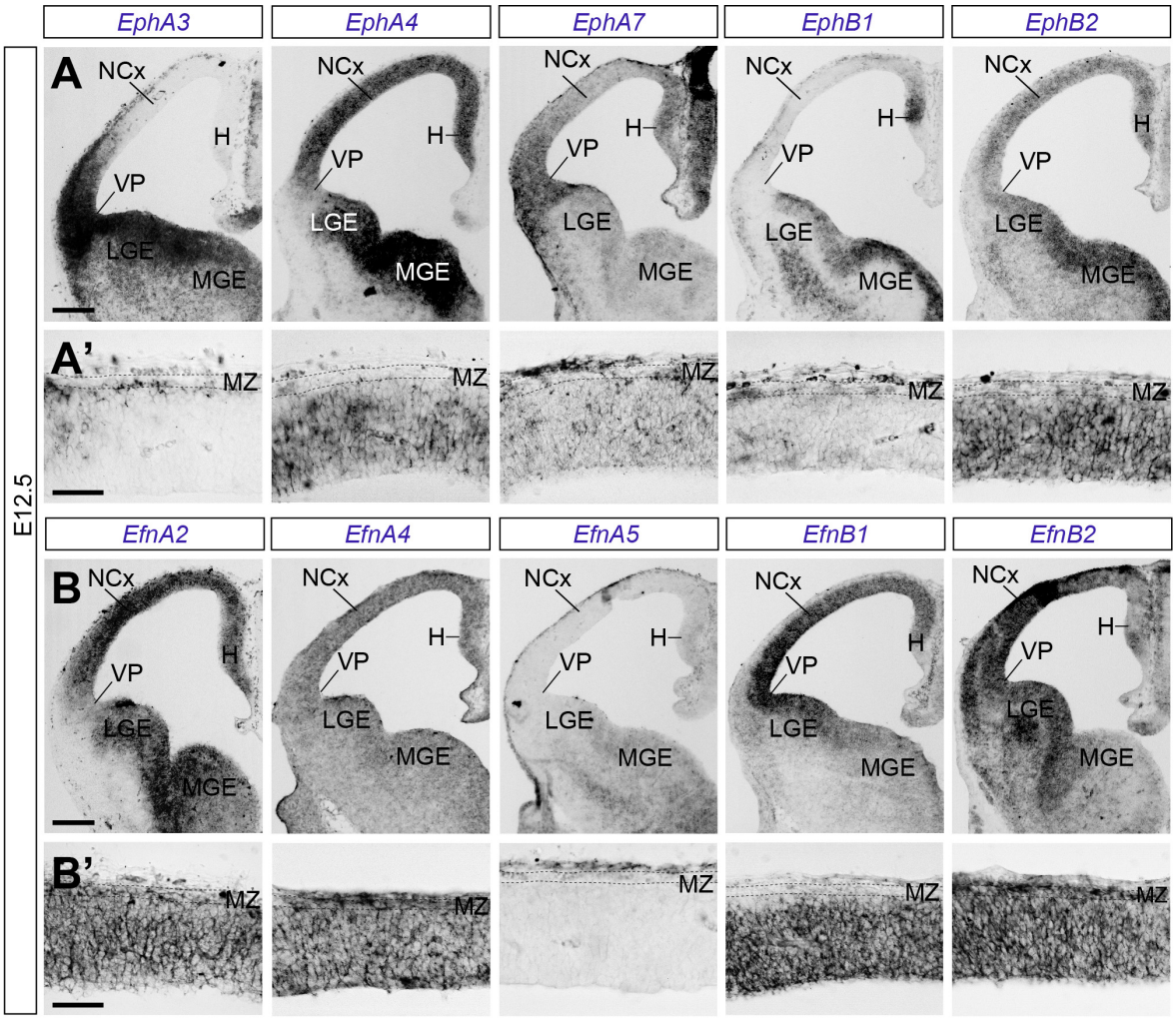

Figure S2. CR cells express multiple Eph receptors and ephrins.

(A and B) Coronal sections through the telencephalon of E12.5 mouse embryos showing the expression of *EphA3*, *EphA4*, *EphA7*, *EphB1*, *EphB2*, *EfnA2*, *EfnA4*, *EfnA5*, *EfnB1* and *EfnB2* mRNA.
(A' and B') Magnification of the neocortex of pictures represented in (A) and (B).
H, hippocampus; LGE, lateral ganglionic eminence; MGE, medial ganglionic eminence; MZ, marginal zone; NCx, neocortex.
Scale bars equal 200 μm (A, B) and 50 μm (A', B').

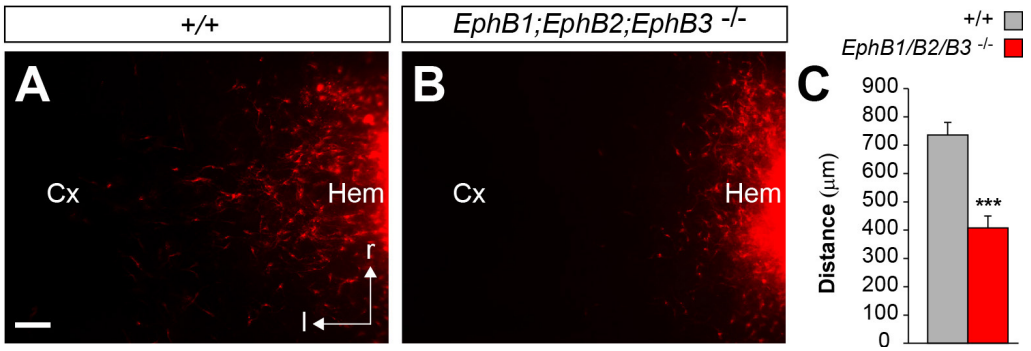

Figure S3. Loss of Eph receptors impairs the dispersion of CR cells throughout the cortex.

(A and B) Representative images of flat whole-mount cortices showing the distribution of wild type (A) and *EphB1/B2/B3* mutant (B) DiI-labeled CR cells.
(C) Quantification of the distance migrated by CR cells in wild type cortices, d = 736.2300 ± 44.0047 μm, and in *EphB1/B2/B3* mutant cortices, d = 409.4888 ± 33.9724 μm. *t*-test, ***p < 0.001, $n = 10$ for each condition.
NCx, neocortex; l, lateral; r, rostral.
Scale bar equals 100 μm.

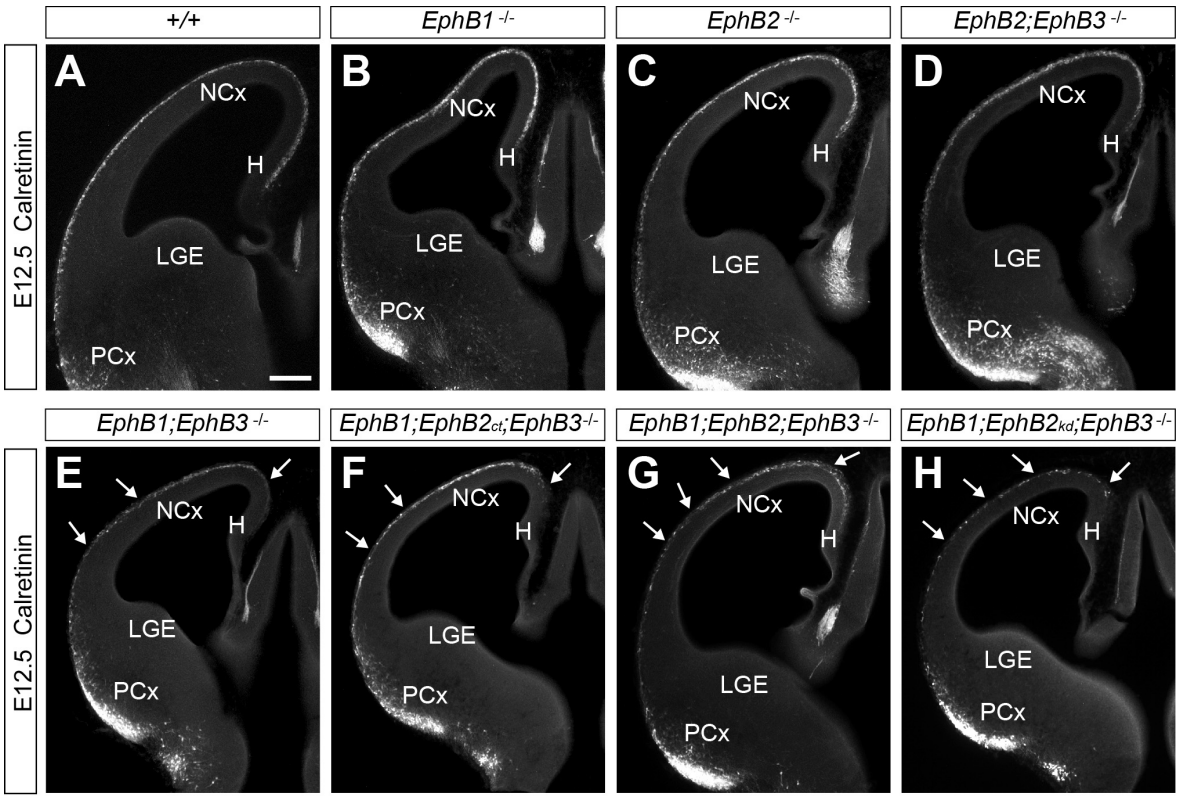

Figure S4. CR cell distribution in an allelic series of *Eph* mutants.

(A to H) Coronal sections through the telencephalon of E12.5 control (A) and *EphB* (B–H) mouse mutant embryos showing the distribution of CR cells by calretinin immunostaining. Note the relatively homogeneous distribution of CR cells in control (A), and *EphB1* (B),

EphB2 (C), and *EphB2;EphB3* (D) mutant embryos. In contrast, CR are abnormally distributed through the surface of the cortex in *EphB1;EphB3* (E) and, even more so, in *EphB1/B2/B3* mutant embryos (F–H). *EphB2*, EphB2$_{ct}$ and EphB2$_{kd}$ are null, carboxyl-deleted and kinase dead alleles of the EphB2 gene, respectively. Arrows point to gaps between CR cells.
LGE, lateral ganglionic eminence; NCx, neocortex; PCx, piriform cortex.
Scale bar equals 200 μm.

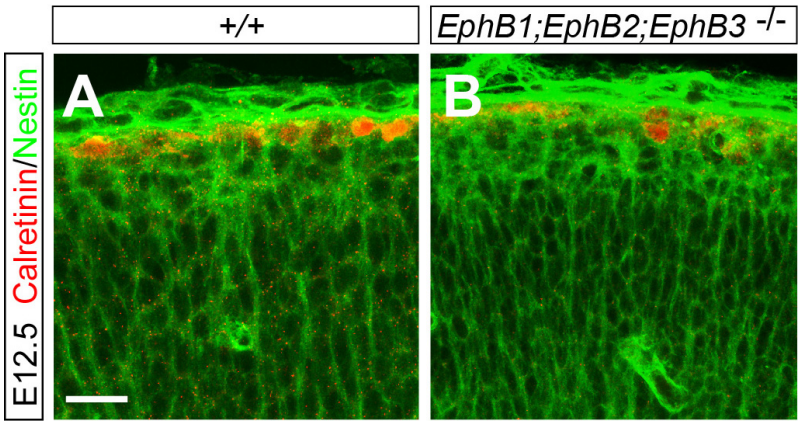

Figure S5. Normal radial glia morphology in *EphB1/B2/B3* mutants.

(A and B) Coronal sections through the cortex of E12.5 control (A) and *EphB1/B2/B3* (B) mouse mutant embryos showing the morphology of the glial palisade by Nestin immunohistochemistry.
CP, cortical plate; MZ, marginal zone.
Scale bar equals 20 μm.

SUPPLEMENTAL MOVIES

Movie S1. CR cell migration in vivo.

Several cells are observed in the surface of the cortex in an intact E13.5 *Calretinin-Cre;RCE* mouse embryo. The blue dot points to a CR cell with a branched leading process that is remodeled as the cell change direction.

Movie S2. Interactions between migrating CR cells.

High-magnification movie showing the interaction between two CR cells in the surface of the cortex in a flat whole-mount preparation at E11.5. Note that upon contact (red arrow), the cell in the right side of the field changes direction, while the leading process of the cell in the left side of the field is retracted.

Movie S3. Dispersion of CR cells away from a hem explant at E12.5.

Low-magnification movie showing the chaotic movement of CR cells as they disperse away from a hem explant. Yellow and red tracks identify the paths followed by two CR cells.

Movie S4. CR cells undergo contact repulsion.

High-magnification movie of a E12.5 hem explant culture in which several CR cells are observed. The red dot identified a migrating CR cell as it interacts with other cells in the field. Note that cell-cell contacts consistently lead to repulsion. The bottom panel illustrates with colored tracks the paths followed by several CR cells.

Movie S5. Directional migration of olfactory bulb interneurons.

High-magnification movie of a E16.5 lateral ganglionic eminence (LGE) explant culture in which several interneurons are observed. Note that interneurons establish cell-cell contacts very frequently, yet they maintain a fairly steady course of migration. The bottom panel illustrates with colored tracks the paths followed by several interneurons.

Movie S6. CR cells undergo contact repulsion.

High-magnification movie of an E11.5 hem explant culture in which several CR cells are observed.

Movie S7. CR cells undergo contact repulsion.

High-magnification movie of an E11.5 pallial septum explant culture in which several CR cells are observed.

Movie S8. Random movement in isolated CR cells.

High-magnification movie of an isolated CR cell that has migrated away from an E12 hem explant. The cell changes its direction of migration at random.

Movie S9. Modeling CR cell migration.

The movie illustrates the modeled behavior of migrating CR cells with or without contact repulsion (CoRe). Note that CR cells undergoing contact repulsion distribute more effectively throughout the field than CR cells in which only random migration is taken into consideration.

Movie S10. Heterotypic interactions between different classes of CR cells.

High-magnification movie showing the interactions between CR cells from two different sources, the hem (green cells) and the pallial septum (transmitted light). Note that CR cells from different sources also undergo contact repulsion. The blue and red dots point CR cells that interact with other CR cells from the same and different source.

Movie S11. Modeling the interactions between CR cells from different sources.

The movie illustrates the modeled behavior of migrating CR cells from two different sources (red and blue), with or without contact repulsion (CoRe). Note that CR cells undergoing contact repulsion distribute more effectively and dynamically stabilize a boundary between the two populations of CR cells. In the absence of contact repulsion, CR cells disperse ineffectively and fail to sustain boundaries.

Movie S12. Blocking Eph/ephrin signaling perturbs contact repulsion between CR cells.

The movie illustrates the migratory behavior of CR cells treated with control Fc or EphA3/B2 Fc fragments. Note that contact repulsion is reduced in EphA3/B2-Fc treated explants compared to controls. CR cells treated with EphA3/B2 Fc fragments tend to sustain their migratory direction and extend longer leading processes than controls.

Movie S13. Defective contact repulsion in CR cells lacking EphB1, EphB2 and EphB3 receptors.

The movie illustrates the migratory behavior of wild type and *EphB1/B2/B3* mutant CR cells. Note that contact repulsion is reduced in the absence of EphB1, EphB2 and EphB3 receptors compared to wild type controls.

SUPPLEMENTAL EXPERIMENTAL PROCEDURES

Mouse strains

Calretinin-Cre mice (Taniguchi et al., 2011) and *Rosa26 Reporter* CAG-boosted EGFP (*RCE*) mice (Sousa et al., 2009) were maintained in a C57BL/6 background, while wild type and ubiquitously expressing GFP mice (Hadjantonakis et al., 1998) were maintained in a CD1 background. The allelic series of *EphB* mutants was generated using different mutations in the *EphB1* gene (Williams et al., 2003), *EphB2* (Birgbauer et al., 2000; Henkemeyer et al., 1996; Hindges et al., 2002) and *EphB3* (Orioli et al., 1996) genes. These mice were maintained in a 129/CD1 mixed background. All control animals used in our experiments were obtained from the same familial genetic background than the corresponding mutant mice. The day of vaginal plug was considered to be embryonic day 0.5 (E0.5). Mice were kept at the Instituto de Neurociencias (Alicante, Spain) in accordance with Spanish and European Union regulations.

Explants, flat whole-mount cultures and in vitro time-lapse imaging

For explant preparations, brain slices were obtained from E12.5 ubiquitously expressing GFP and wild type mice as described previously (Anderson et al., 1997). Hem, pallial septum (PS) and ventral pallium (VP) explants were dissected from organotypic slices of ubiquitously expressing GFP embryos (hem and PS) or *Calretinin-Cre* embryos (VP), and cultured on glass coverslips (BD BioCoat™ Poly-L-Lysine 12 mm) coated with laminin in Neurobasal medium containing 0.4% of methylcellulose (Sigma). The large majority of cells produced by hem (Borrell and Marín, 2006) or PS (93.4% Reelin+ cells, $n = 516$ cells from 5 different experiments) explants were found to be CR cells. In blocking experiments, explants were treated with EfnA1-Fc, EfnB1-Fc, EphA3-Fc or EphB2-Fc fragments alone (10 μg/ml, R&D Systems), with a mix of EphA3-Fc and EphB2-Fc fragments (10 μg/ml of each proteins, R&D Systems), or with human IgG Fc fragments (10 μg/ml or 20 μg/ml, Jackson ImmunoResearch) as control.

For flat whole-mount preparations, the neocortex of E11.5 and E12.5 wild type, control or *EphB1/B2/B3* mutant embryos was dissected from the telencephalon and flat mounted on culture plate inserts (Millipore). For transplantation assays, hem explants from E12.5 GFP-expressing embryos were subsequently transplanted into E11.5 or E11.5 wild type flat cortices, and the compound preparations were cultured in Neurobasal for 48h. For experiments with control and *EphB1/B2/B3* mutant embryos, small DiI crystals

were inserted in the hem of the flattened cortices to label CR cells and cultured as in transplantation assays.

For time-lapse imaging, coverslips and plate inserts were transferred to a glass bottom microwell dish with the same medium and placed in the stage of an inverted Leica laser scanning spectral confocal microscope TCS SP2 AOBS. Samples were maintained at 37ºC with 5% CO_2 during the experiment. We used a 488 laser to acquire the emission of GFP at 500-550 nm, and transmitted light with 20-40x dry objectives. Cell-cell contacts were identified through three-dimensional analysis with Imaris® software.

Imaging CR cell migration in vivo

Pregnant mice carrying E12.5 or E13.5 *Calretinin-Cre;RCE* mouse embryos were anesthetized with isofluorane for the surgery. After laparotomy, an individual embryo was placed in a dish located just above the mother through a silicon hole. The embryo was then fixed to the plate with 4% agarose to avoid body movements; only the superior part of the head was devoid of agarose and covered with heated PBS. Time-lapse imaging of CR cells (identified by the expression of GFP from the Calretinin locus) migrating along the marginal zone was recorded with a Leica laser scanning spectral confocal microscope TCS SP2 RS (resonant scanning) using long working distance and water immersion 10-20x objectives. EGFP was excited at 488 nm and acquired at 500-550 nm.

In situ hybridization and immunohistochemistry

For in situ hybridization (ISH), brains were fixed overnight in 4% paraformaldehyde in PBS. Twenty-micrometer frozen sections were hybridized with digoxigenin-labeled probes, as described before (Flames et al., 2007).

Immunohistochemistry was performed on vibratome sections and hem explants, as described before (Flames et al., 2007; López-Bendito et al., 2008), using chicken anti-GFP (1:1000, Aves Labs) and rabbit anti-Calretinin (1:3000, Swant) antibodies. The secondary antibodies were goat anti-chicken 488 and donkey anti-rabbit 555 (1:200, Molecular Probes). DAPI (Sigma) was used for fluorescent nuclear staining.

For the detection of Eph and ephrins in the surface of CR cells, we incubated live hem explants with Eph-Fc or ephrin-Fc ectodomains at 37°C during 5 min. After rinsing the Fc fragments, we incubated the explants for 1h with goat anti-human Fc (1:500, Jackson ImmunoResearch), followed by 30 min with donkey anti-goat 594 antibodies (1:200, Molecular Probes). To prevent receptor internalization, both incubation steps were performed at 4ºC without permeabilization.

Quantification

The analysis of the tracks of migrating CR cells as well as the area occupied by CR cells in the surface of the cortex was carried out using ImageJ software. To calculate the area occupied by CR cells, we used coronal sections through rostral, intermediate and caudal levels through the cortex of E12.5 wild type and *EphB1/B2/B3* knockout mouse embryos ($n = 6$). We set an arbitrary threshold for signal intensity to quantify the distribution of CR cells. For each level, we quantified the percentage of area occupied by CR cells from the total area of the neocortex, and a mean value for each brain was subsequently obtained.

The directionality index was calculated as the net displacement of a cell divided by the total path length followed by the cell. Velocity vectors and angles after collision were calculated using Matlab software. For the quantification of the P/D ratio in explants, the distance migrated by the 30 furthest cells was measured in the proximal and distal side of each explant using Neurolucida Explorer (MBF Bioscience) software.

For the analysis of the distance migrated by CR cells in flat cortices, we measured the distance migrated by the 50 furthest cells in transplanted cortices and the distance migrated by the 20 furthest DiI-labeled cells in wild type and *EphB1/B2/B3* knockout mice cortices, using Neurolucida Explorer (MBF Bioscience) software.

All quantifications represent mean ± standard error of the mean (SEM).

Model

The model consists of a single layer representing the cortical surface. To simulate the tangential migration and final distribution of CR cells in the developing cortex we adopted a strategy based on random movement of individual neurons and repulsion upon contact between neighboring cells.

Tangential migration. To quantify the movement of CR cells along the cortical surface, we measured space and time in arbitrary units, pixels and frames respectively. Each cycle of the stochastic model is divided in 5000 frames of arbitrary duration. The velocity module of individual CR cells was chosen randomly from a distribution ranging from 0.5 to 1.5 pixels/frame and it remained constant throughout the entire modeling cycle (similar results were obtained with different distributions; data not shown).

The initial direction of motion for each CR cell was independently determined at random and updated every frame depending on its interactions with other cells. In the case of no interaction, the new direction was again chosen at random from all possible directions that maintain the velocity module unchanged. If during the preceding frame the reference CR cell A entered in contact with at least another CR cell, then the new direction (ND) of motion was computed according to an interaction function defined by the weighted sum of the individual vectors that linked CR cell A to all other CR cells within a radius of 7 pixels (similar results were obtained with smaller or larger neighborhoods; data not shown). The weights were calculated with an exponential distribution that depends on distance from A

$$ND = \sum_{Ci \in S} \exp\left(\frac{-d_i}{2 * \sigma^2}\right) * (P - p_i)$$

here S is the group of all CR cells within a radius of 7 pixels from A; d_i is the distance between A and cell C_i; P and p_i are the positions of A and C_i, respectively; and sigma was set such that the weight of a CR cell located exactly 7 pixels away from A was 0.01.

Minimum distance. We used minimum average distance from every pixel in the cortical model to its closest CR cell as a measure of cortical coverage and regularity. Non-random, regular mosaics minimize the variance and the minimum average distance to guarantee uniform and optimal coverage.

Regularity index. We used the regularity index to analyze coverage homogeneity. The regularity index is the result of dividing the average Voronoi domain area by the standard deviation (std). The Voronoi domain of one cell is the area that contains the points in the plane that are closer to that cell than to any other cell.

Segregation index. For every position X in the cortical model, we calculated the influence of each population of CR cells, S1 and S2, as

$$I = \sum_{Ci \in S} \exp\left(\frac{-d_i}{2 * \sigma^2}\right)$$

here d_i is the distance between position X and cell C_i; and sigma was set to 10 (similar results were obtained with smaller or larger neighborhoods; data not shown).

After obtaining a spatial map of the influence of each population of CR cells, M1 and M2, we computed the segregation index as

$$SI = \frac{abs(M_1 - M_2)}{M_1 + M_2}$$

For graphical purposes, in Figs 2a and 2o, the maps were collapsed along the vector joining the sources of the two CR cell populations (cortical space was divided in 10 bins).

For minimum distance quantification *in vivo*, we performed a mask with the position of Reelin positive cells in whole mounted brains using ImageJ software. We obtained the position coordinates of each dot in the mask and we quantified the minimum distance using Matlab software (see above).

To discriminate the contribution of cell number and contact repulsion to the final distribution of CR cells, we performed *in silico* experiments using our mathematic model. In brief, we first inferred the number of CR cells in wild type and *EphB1/B2/B3* mutant cortices by analyzing their area coverage. To simulate the different sources of CR cells in vivo, we placed 65% of these cells in one side of the rectangle (putative hem derive CR cells), 35% in the opposite side (putative PSB derived CR cells) and 5% (putative PS derived CR cells) in the upper side. We then run the model using the corresponding number of cells found in wild type or *EphB1/B2/B3* mutant rectangular masks with or without contact repulsion. In brief, we simulate four experimental conditions: (1) normal number of cells with contact repulsion (equivalent to wild type condition), (2) reduced number of cells without contact repulsion (equivalent to mutant condition), (3) normal number of cells without contact repulsion (equivalent to a situation in which contact repulsion would be irrelevant for the distribution of CR cells), and (4) reduced number of cells with contact repulsion (equivalent to a situation in which the number of cells would be irrelevant for the distribution of CR cells). We quantified the minimum distance for all four experimental conditions. Cross-comparisons between these four conditions led to the conclusion that both cell number and contact repulsion are likely responsible for the abnormal distribution of CR cells in *EphB1/B2/B3* mutants.